Commun. Comput. Phys.
doi: 10.4208/cicp.070709.011209a

Vol. **8**, No. 2, pp. 445-470
August 2010

A Technique for High-Order Treatment of Diffusion Terms in Semi-Lagrangian Schemes

Roberto Ferretti*

Dipartimento di Matematica, Università di Roma Tre, L.go S. Leonardo Murialdo, 1, 00146 Roma, Italy.

Received 7 July 2009; Accepted (in revised version) 1 December 2009

Communicated by Chi-Wang Shu

Available online 7 April 2010

Abstract. We consider in this paper a high-order, semi-Lagrangian technique to treat possibly degenerate advection-diffusion equations, which has been proposed in similar forms by various authors. The scheme is based on a stochastic representation formula for the solution, which allows to avoid the splitting between advective and diffusive part of the evolution operator. A general theoretical analysis is carried out in the paper, with a special emphasis on the possibility of using large Courant numbers, and numerical tests in one and two space dimensions are presented.

AMS subject classifications: 65M25, 65M12, 60H30

Key words: Advection-diffusion equations, stochastic representation, method of characteristics, semi-Lagrangian schemes, high-order schemes, convergence.

1 Introduction

This paper is devoted to a semi-Lagrangian type treatment of second order terms in advection-dominated, possibly degenerate, parabolic equations. Although several extensions are possible, we will use the advection-diffusion equation,

$$\begin{cases} v_t(x,t) = \sum_{i,j=1}^{N} a_{ij} \dfrac{\partial^2}{\partial x_i \partial x_j} v(x,t) + f(x) \cdot \nabla v(x,t) + g(x), \\ v(x,0) = v_0(x), \end{cases} \tag{1.1}$$

(with $x \in \mathbb{R}^N$, $t \in [0,T]$, v_0 compactly supported in $\mathbb{R}^N$) as a model problem to describe the technique and to carry out a general convergence analysis. Here, we assume that

*Corresponding author. *Email address:* ferretti@mat.uniroma3.it (R. Ferretti)

$A=(a_{ij})\in\mathbb{R}^{N\times N}$ is a positive semidefinite matrix, thus including degenerate second-order operators. In order to have more explicit results, we will possibly assume in the sequel that the advection term is driven by a constant vectorfield:

$$f(x)\equiv\begin{pmatrix}f_1\\ \vdots\\ f_N\end{pmatrix}. \tag{1.2}$$

The semi-Lagrangian (SL) schemes stem from the so-called Courant-Isaacson-Rees scheme (see [5]), and at the moment they are very popular in the Numerical Weather Prediction community. In this setting, they have been introduced by Wiin-Nielsen in [26] and brought to the present form by Robert in the 80s (see [23] and the review paper [25]). In a partly independent way, SL schemes have also been proposed in [4] and widely applied to plasma physic problems since (see, e.g., [14, 24]).

The general idea of SL methods is to reconstruct the solution by integrating numerically the equation along the characteristics starting from any grid point, not over the whole time interval (as it would be the case in the particle method), but over a single time step. The scheme is constructed by coupling a numerical method for ODEs (to compute the upwind points with respect to the grid nodes) with an interpolation formula (to recover the value of the solution in such points, which are not in general grid points themselves). The comparison with more classical Eulerian difference schemes shows that in general SL schemes have a higher computational cost per time step, but that they also allow for larger time steps.

If $A=0$ (i.e. in the case of pure advection), the schemes rely on the representation formula

$$v(x,t)=\int_0^t g(y(s))ds+v_0(y(t)), \tag{1.3}$$

where $y(t)$ is the solution of

$$\begin{cases}\dot{y}(s)=f(y(s)),\\ y(0)=x.\end{cases} \tag{1.4}$$

Although using the representation formula (1.3) is very natural in the case of (linear) first order equations, the situation gets more complex when a diffusion term appears. In this situation, the usual response is to split the evolution operator and treat in semi-Lagrangian way only the first order part. This results either in very severe time-step bounds, or in the additional computational effort of solving an implicit scheme for the second order term, with the further drawback that the splitting itself introduces a limitation in the consistency rate of the scheme. A second approach is related to the so-called Lagrange-Galerkin schemes (proposed independently in [7] and [22]) which however cannot be exactly implemented in general (see [21]).

On the other hand, a natural extension of the technique used for pure advection equations can be provided by the stochastic representation (Feynman-Kac) formula for the

solution of (1.1):

$$v(x,t)=\mathbb{E}\left\{\int_0^t g(y(s))ds+v_0(y(t))\right\}, \tag{1.5}$$

where $y(t)=y(x,t)$ is now the solution of the stochastic differential equation (SDE):

$$\begin{cases} dy(s)=f(y(s))ds+\sqrt{2}BdW, \\ y(0)=x. \end{cases} \tag{1.6}$$

In (1.6), B is a matrix such that $BB^t=A$ and $\mathbb{E}\{\cdot\}$ is the expectation with respect to the Wiener measure (i.e. the probability measure of the Brownian process W in (1.6)). The solution of (1.6) must be understood in the Ito sense (although of course in the case of constant B as in (1.1) it coincides with the solution in the Stratonovich sense). Typically, the representation formula (1.5)-(1.6) may be applied for any bounded and uniformly continuous solution v of (1.1), despite of the possible degeneracy of the second-order operator. This leads to consider solutions of (1.1) in the viscosity sense (see [6]), although different analytical tools have been developed for such problems.

Note that if the parabolic operator is nondegenerate, then the matrix A has full rank and the factor B must be a $N\times N$ matrix (for instance, a Cholesky factor of A). If the operator is degenerate along $N-M$ directions, then B might be constructed to have dimension $N\times M$ (such an example will be considered in the section on numerical tests). It is also easy to see that if $A=0$, then (1.5) reduces to (1.3).

The use of the Feynman-Kac formula for numerical purposes was first proposed by Kushner in the 70s (see [16] for an up-to-date review) in the field of stochastic Dynamic Programming equations, which of course include problem (1.1). Kushner's approach results in a first order, Eulerian scheme. A first order, SL scheme have then been proposed in [2], in which use of the Feynman-Kac formula is blended with large time-step techniques. Independently, the same approach was proposed in [18–20] and developed in a series of papers, mainly focused on semilinear parabolic equations and Fluid Dynamics problems. In this latter line of research, high-order discretizations are considered with respect to time but not to space, and although the case of large Courant number is considered, still the interaction between the two discretizations remains essentially unclear. We mention that a similar technique is also considered in [27] with a specific focus on degenerate elliptic equations, and that techniques of stochastic derivation have been successfully applied to degenerate nonlinear second order equations, in particular the equation of Mean Curvature Motion (see [3,9] and the references therein).

The purpose of this paper is to analyse (in the simplified setting of linear advection-diffusion equations) a general version, high-order both in time and space, of the above schemes. To this end, we will make extensive use of the theory of weak approximation for Stochastic Differential Equations, along with the convergence results obtained for the first-order advection equation. Consistency and stability, as well as the behaviour of the numerical domain of dependence, will be studied in a form as independent as possible of the relationship between discretization steps. The effectiveness of this approach will be

discussed with an accent on the possibility of using large Courant numbers, which characterizes SL schemes. We explicitly point out that the analysis carried out in the paper can in principle be applied to more general advection-diffusion equations (in particular, with nonconstant coefficients), although in practice this may result in an overly complex scheme.

The outline of the paper is the following. Section 2 reviews some basic approximation results for Stochastic Differential Equations. Section 3 deals with time and space discretization, whereas in Section 4 we carry out a general consistency and stability analysis, and a Fourier analysis of the scheme for the simplified one-dimensional, constant coefficient case. Finally, we study in Section 4 the behaviour of the numerical domain of dependence under large Courant numbers, and present in Section 5 the results of some numerical tests in $\mathbb{R}^1$ and $\mathbb{R}^2$.

2 Approximation of Stochastic Differential Equations

We will review in this section some useful points in the theory of approximation for SDEs. For an extensive treatment of the problem, the reader is referred to [15, 17].

To fix ideas, we assume that the functions $f:\mathbb{R}^N\to\mathbb{R}^N$ and $g:\mathbb{R}^N\to\mathbb{R}$ are bounded along with their derivatives, up to the order required by the desired consistency rate.

The approximation of the SDE (1.6) is a widely studied problem in probability theory. It turns out that (1.6) can be approximated at least in two different senses. *Strong* convergence (with order p) means that, using in the numerical scheme suitable increments of a particular trajectory of the Brownian process, the numerical trajectory of (1.6) converges in probability to the exact trajectory (with order p), that is

$$\mathbb{E}\{|y_k-y(k\Delta t)|\}\to 0 \qquad (\mathbb{E}\{|y_k-y(k\Delta t)|\}\le \Delta t^p), \tag{2.1}$$

whereas *weak* convergence means that the same holds only for expected values, that is

$$|\mathbb{E}\{h(y_k)\}-\mathbb{E}\{h(y(k\Delta t))\}|\to 0 \qquad (|\mathbb{E}\{h(y_k)\}-\mathbb{E}\{h(y(k\Delta t))\}|\le \Delta t^p). \tag{2.2}$$

for any smooth function h, and any k such that $0\le k\Delta t\le T$ (we have denoted by $|\cdot|$ a given norm in $\mathbb{R}^N$). In general, it happens that the convergence rate of the approximation is higher for weak approximations. Moreover, under suitable assumptions, the averaging of the trajectories in (2.2) (which is in principle a Monte Carlo type algorithm) needs only to be computed on a limited number of trajectories, this number depending on the order of the scheme.

Since our interest is in computing the expectation in (1.5), we will focus on weak approximations. The examples in Table 1 (which are all from [15]) show the stochastic versions of some well known one-step schemes. Here, FE and BE stand for respectively Forward and Backward Euler, H for Heun and CN for Crank-Nicolson. Clearly, obtaining the maximum convergence rate for the scheme requires suitable regularity assumptions on the various terms of the SDE. This work, however, is not focused on a particular recipe

Table 1: Stochastic explicit and implicit first- and second-order schemes.

scheme	**form**	**order**
FE	$y_{k+1}=y_k+\Delta t f(y_k)+\sqrt{2}B\Delta W_k$	$p=1$
BE	$y_{k+1}=y_k+\Delta t f(y_{k+1})+\sqrt{2}B\Delta W_k$	$p=1$
H	$y_{k+1}=y_k+\frac{\Delta t}{2}(f(y_k)+f(y_k+\Delta t f(y_k)+\sqrt{2}B\Delta W_k))+\sqrt{2}B\Delta W_k$	$p=2$
CN	$y_{k+1}=y_k+\frac{\Delta t}{2}(f(y_k)+f(y_{k+1}))+\sqrt{2}B\Delta W_k$	$p=2$

and therefore, in what follows, we will simply assume (2.2) (possibly, for some order p), with the standing hypothesis that data are smooth enough for it to hold.

Although the increments ΔW_k should be understood as vectors of independent gaussian variables with zero mean and variance Δt, in practice (see [15,17]) in order to achieve first order weak convergence in Euler schemes it suffices to use for any component $\Delta W_{k,i}$ of ΔW_k, a two-point distributed variable with probability density

$$P(\Delta W_{k,i}=\pm\sqrt{\Delta t})=\frac{1}{2}, \tag{2.3}$$

whereas second order weak convergence for Heun and Crank-Nicolson schemes may be achieved provided the variables $\Delta W_{k,i}$ satisfy for example

$$P(\Delta W_{k,i}=\pm\sqrt{3\Delta t})=\frac{1}{6},\quad P(\Delta W_{k,i}=0)=\frac{2}{3}. \tag{2.4}$$

Probability density for the whole vector ΔW_k is then obtained by product of independent one-dimensional densities. For instance, in two space dimensions, (2.3) would result in the discrete probability distribution

$$\begin{aligned} &P\left(\Delta W_k=\begin{pmatrix}+\sqrt{\Delta t}\\ +\sqrt{\Delta t}\end{pmatrix}\right)=P\left(\Delta W_k=\begin{pmatrix}+\sqrt{\Delta t}\\ -\sqrt{\Delta t}\end{pmatrix}\right)\\ =P&\left(\Delta W_k=\begin{pmatrix}-\sqrt{\Delta t}\\ +\sqrt{\Delta t}\end{pmatrix}\right)=P\left(\Delta W_k=\begin{pmatrix}-\sqrt{\Delta t}\\ -\sqrt{\Delta t}\end{pmatrix}\right)=\frac{1}{4}. \end{aligned} \tag{2.5}$$

In general, higher order schemes may be constructed either by some generalization of deterministic schemes, or by extrapolation on second or third order schemes (see [15] for details). In both cases, the increase in computational complexity may be considerable.

3 Time and space discretization

We will first obtain in this section a discrete time approximation of the representation formula (1.5), by a stochastic one-step time discretization of order $p\geq 1$, in the form:

$$\begin{cases} y_{k+1}=y_k+\Delta t\Phi(y_k,y_{k+1},\Delta W_k)\\ y_0=x. \end{cases}$$

Table 2: Stochastic first- and second-order schemes for the augmented system (3.1).

scheme	form
FE	$\Phi_f(x,\bar{y},\Delta W)=f(x)+\sqrt{2}B\Delta W$ $\Phi_g(x,\bar{y},\Delta W)=g(x)$
BE	$\Phi_f(x,\bar{y},\Delta W)=f(\bar{y})+\sqrt{2}B\Delta W$ $\Phi_g(x,\bar{y},\Delta W)=g(\bar{y})$
H	$\Phi_f(x,\bar{y},\Delta W)=\frac{1}{2}(f(x)+f(x+\Delta t f(x)+\sqrt{2}B\Delta W))+\sqrt{2}B\Delta W$ $\Phi_g(x,\bar{y},\Delta W)=\frac{1}{2}(g(x)+g(x+\Delta t f(x)+\sqrt{2}B\Delta W))$
CN	$\Phi_f(x,\bar{y},\Delta W)=\frac{1}{2}(f(x)+f(\bar{y}))+\sqrt{2}B\Delta W$ $\Phi_g(x,\bar{y},\Delta W)=\frac{1}{2}(g(x)+g(\bar{y}))$

Following [8], it is convenient to consider the dynamical system:

$$\begin{pmatrix} dy(s) \\ d\gamma(s) \end{pmatrix} = \begin{pmatrix} f(y(s))ds+\sqrt{2}BdW \\ g(y(s))ds \end{pmatrix} \tag{3.1}$$

with the initial conditions $y(0)=x$, $\gamma(0)=0$. Applying a stochastic one-step scheme to (3.1), and restricting to the first time step, we have:

$$\begin{pmatrix} \bar{y} \\ \bar{\gamma} \end{pmatrix} = \begin{pmatrix} x \\ 0 \end{pmatrix} + \Delta t \begin{pmatrix} \Phi_f(x,\bar{y},\Delta W) \\ \Phi_g(x,\bar{y},\bar{\gamma},\Delta W) \end{pmatrix} \tag{3.2}$$

where we split the function Φ according to (3.1). In (3.2), $\bar{y}$ is an approximation of $y(\Delta t)$, whereas $\bar{\gamma}$ approximates the integral between 0 and Δt in (1.5) (note that the diffusion appears only in the components of y). If an implicit scheme is used, $\bar{y}$ and $\bar{\gamma}$ are understood as the solutions of equation (3.2). In any case, we will sometimes use in the sequel the notations $\bar{y}(x,\Delta W)$ or $\bar{\gamma}(x,\Delta W)$ to denote the left-hand side of (3.2). In order to clarify the previous construction, we rewrite in Table 2 the schemes of Section 2 in the form (3.2). Note that all the scheme still keep the same weak convergence rate in this version.

3.1 Time-discrete scheme

If we denote by $\bar{v}^k$ a time-discrete approximate solution at time $t_k=k\Delta t$, obtained rewriting (1.5) on a single time step and introducing the previous one-step approximation of (1.6), we obtain:

$$\bar{v}^{k+1}(x)=\mathbb{E}\left\{\bar{\gamma}(x,\Delta W)+\bar{v}^k(\bar{y}(x,\Delta W))\right\}. \tag{3.3}$$

Now, relying on the assumption of weak convergence, we further compute the expectation with respect to ΔW by working on a "small" number of realisations as shown in Section 2. We associate a weight w_i to a realisation Δ_i of the variable ΔW so as to have

$$P(\Delta W=\Delta_i)=w_i \quad (i=1,\cdots,s) \tag{3.4}$$

with the obvious conditions

$$w_i \geq 0, \quad \sum_{i=1}^{s} w_i = 1 \tag{3.5}$$

and the further assumptions (see [15]):

$$\sum_{i=1}^{s} w_i \Delta_i = 0, \tag{3.6}$$

$$\sum_{i=1}^{s} w_i \Delta_i^2 = \Delta t \tag{3.7}$$

(this latter condition should be understood in one dimension, and extended to multiple dimensions as in (2.3), (2.5)).

Using the discrete probability density (3.4) in (3.3), we obtain a second time-discrete approximation in the form

$$v^{k+1}(x) = \sum_{i=1}^{s} w_i \left\{ \bar{\gamma}(x,\Delta_i) + v^k(\bar{y}(x,\Delta_i)) \right\} \tag{3.8}$$

in which the initial condition $v^0(x)$ for $k=0$ coincides with $v_0(x) = v(x,0)$.

3.2 Fully discrete scheme

The following step to obtain a fully discrete scheme is to discretize (3.8) with respect to space variables, by setting up a space grid in the computational domain. Although unnecessary in principle, we will assume that the grid is orthogonal and uniform, with space step Δx and nodes $x_j = j\Delta x$, for a multiindex $j \in \mathbb{Z}^N$). We denote by v_j^k be the desired approximation of $v(x_j,t_k)$, by V^k and U (respectively, $U(t)$) the set of nodal values of respectively the numerical solution at time t_k and of a generic function $u(x)$ (respectively, $u(x,t)$).

In particular, if $N=1$, nodal values are represented as infinite vectors of samples so that

$$\begin{aligned} V^k &:= \begin{pmatrix} \cdots & v_{-1}^k & v_0^k & v_1^k & \cdots \end{pmatrix}^t, \\ U &:= \begin{pmatrix} \cdots & u(x_{-1}) & u(x_0) & u(x_1) & \cdots \end{pmatrix}^t, \\ U(t) &:= \begin{pmatrix} \cdots & u(x_{-1},t) & u(x_0,t) & u(x_1,t) & \cdots \end{pmatrix}^t. \end{aligned}$$

Then, (3.8) is computed at each node, replacing the "upwind" value $v^k(\bar{y}(x,\Delta_i))$ with a suitable polynomial reconstruction $I[V^k](x)$ such that $I[U](x_j) = u_j$, and if $u(x)$ is a function of $W^{r,\infty}$ then, for any x,

$$|I[U](x) - u(x)| \leq C\Delta x^r. \tag{3.9}$$

Practical examples of reconstruction operators include Lagrange, monotonic or non-oscillatory nonlinear interpolations, as well as finite element reconstructions which would also allow for an unstructured grid. In all such situations, $r=m+1$, where m represents the order of the interpolating polynomial (we will assume in the sequel that $m\geq 1$, so that constant and linear functions are reconstructed with no interpolation error).

The fully discrete scheme may finally be written as

$$\begin{cases} v_j^{k+1}=\sum_{i=1}^{s} w_i\left\{\bar{\gamma}(x_j,\Delta_i)+I[V^k](\bar{y}(x_j,\Delta_i))\right\}, \\ v_j^0=v_0(x_j), \end{cases} \tag{3.10}$$

or, in a compact form,

$$V^{k+1}=S^{\Delta x,\Delta t}(V^k). \tag{3.11}$$

Remark 3.1. Note that (3.10) shows that the computational complexity of the complete scheme is s times the complexity of the inviscid version. The factor s can be quite large, however — typically $s=2^N$ for first order schemes, $s=3^N$ for second order schemes, in case of nondegenerate diffusions. Nevertheless, the overall complexity of the scheme remains linear with respect to the number of points in the space-time grid, so that (at least asymptotically) it has the lowest possible growth rate. Moreover, situation improves in case of degenerate diffusions.

4 Convergence and error analysis

In examining the convergence of the fully discrete scheme (3.10), we should take into account that convergence theory for SL schemes applied to first-order equations is itself somewhat incomplete. More precisely (see [1, 8, 11]), the unconditional stability of SL schemes, which is a widely observed fact in practice, has only been theoretically proved for the case of constant coefficient equation (although an extension to more general linear equations is in progress [12]). In what follows, the convergence analysis will be performed in a normalized Hölder norm, so that

$$\|V\|_\alpha := \begin{cases} \left(\Delta x^N \sum_j |v_j|^\alpha\right)^{1/\alpha}, & \text{if } \alpha<\infty, \\ \max_j |v_j|, & \text{if } \alpha=\infty. \end{cases}$$

We recall that setting $A=0$ in (1.1), we obtain the first order advection equation

$$\begin{cases} v_t(x,t)=f(x)\cdot\nabla v(x,t)+g(x), \\ v(x,0)=v_0(x). \end{cases} \tag{4.1}$$

Accordingly, we could define a family of inviscid schemes in the form

$$u_j^{i,k+1}=\bar{\gamma}(x_j,\Delta_i)+I[U^{i,k}](\bar{y}(x_j,\Delta_i)), \tag{4.2}$$

with $U^{i,k}$ set of nodal values associated to the scheme (4.2) and to Δ_i, in particular

$$U^{i,k}=\begin{pmatrix}\cdots & u_{-1}^{i,k} & u_0^{i,k} & u_1^{i,k}\cdots\end{pmatrix}^t,$$

if $N=1$. Then, the SL scheme for (4.1) corresponds to the case $\Delta_i=0$, and a time step of the scheme (3.10) is performed by a convex combination of schemes in the form (4.2).

4.1 Stability

It is immediate to show that the scheme (3.10) is stable provided its inviscid counterparts (4.2) are stable, as stated by the following result.

Theorem 4.1. *Let the family of schemes* (4.2) *be L^α-stable for any $i\in[1,\cdots,s]$, that is*

$$\|U^{i,k+1}\|_\alpha\le(1+C\Delta t)\|U^{i,k}\|_\alpha \tag{4.3}$$

for a positive constant C independent of Δx, Δt. Then,

$$\|V^{k+1}\|_\alpha\le(1+C\Delta t)\|V^k\|_\alpha \tag{4.4}$$

with V^k solution of (3.10).

Proof. Define

$$\bar v_j^{i,k+1}=\bar\gamma(x_j,\Delta_i)+I[V^k](\bar y(x_j,\Delta_i)) \tag{4.5}$$

with $\bar V^{i,k+1}=(\bar v_1^{i,k+1}\cdots\bar v_q^{i,k+1})^t$. Then, the scheme (3.10) may be written as

$$v_j^{k+1}=\sum_{i=1}^s w_i\bar v_j^{i,k+1}.$$

Using (4.5) and (3.5), we get therefore

$$\|V^{k+1}\|_\alpha\le\sum_{i=1}^s w_i\|\bar V^{i,k+1}\|_\alpha\le\sum_{i=1}^s w_i(1+C\Delta t)\|V^k\|_\alpha,$$

which, by (3.5), coincides with (4.4). □

Remark 4.1. Relating stability of (3.10) to the stability of (4.2) allows to apply at least two theoretical frameworks:

- Low order ($\mathbb{P}_1$, $\mathbb{Q}_1$) space reconstructions for which the inviscid scheme is monotone and therefore L^∞ stable (in fact, the complete scheme (3.10) is also monotone in this case);
- Constant coefficient equations obtained assuming (1.2). In this case, two kind of stability proof have been given for the inviscid case:

– Von Neumann analysis in one space dimension as proved in [8], [1] for Lagrange reconstructions. We mention that, in the line of Von Neumann analysis, a first result on finite element reconstruction has been proved in [13].
– Equivalence between the SL scheme and a stable Lagrange-Galerkin scheme. This technique has been recently proposed in [11] in the situation of high-order Lagrange reconstructions of odd degree, or interpolatory wavelets, in multiple space dimensions. Its extension to the nonconstant coefficient advection equation (4.1) is in progress (see [12]).

4.2 Consistency

The second part in the study of convergence is given by the consistency estimate which follows.

Theorem 4.2. *Let f be a smooth vector field, g be a smooth bounded function, $v(\cdot,\cdot)$ be a smooth solution of* (1.1). *Assume moreover that* (2.2) *and* (3.9) *hold. Then the local truncation error satisfies the bound*

$$\frac{1}{\Delta t}\left\| V(t_{k+1}) - S^{\Delta x,\Delta t}(V(t_k)) \right\|_\alpha \le C\left(\Delta t^p + \frac{\Delta x^r}{\Delta t}\right). \tag{4.6}$$

Proof. We estimate a single component in the left-hand term of (4.6) as

$$\begin{aligned}
&\frac{1}{\Delta t}\left| v(x_j,t_{k+1}) - \sum_{i=1}^{s} w_i\{\bar\gamma(x_j,\Delta_i) + I[V(t_k)](\bar y(x_j,\Delta_i))\}\right| \\
&\le \frac{1}{\Delta t}\left| v(x_j,t_{k+1}) - \sum_{i=1}^{s} w_i\{\bar\gamma(x_j,\Delta_i) + v(\bar y(x_j,\Delta_i),t_k)\}\right| \\
&\quad + \frac{1}{\Delta t}\left| \sum_{i=1}^{s} w_i\{\bar\gamma(x_j,\Delta_i) + v(\bar y(x_j,\Delta_i),t_k)\} - \sum_{i=1}^{s} w_i\{\bar\gamma(x_j,\Delta_i) + I[V(t_k)](\bar y(x_j,\Delta_i))\}\right|.
\end{aligned} \tag{4.7}$$

We recall that the representation formula (1.5) gives for $v(x_j,t_{k+1})$:

$$v(x_j,t_{k+1}) = \mathbb{E}\left\{ \int_0^{\Delta t} g(y(x_j,s))ds + v(y(x_j,\Delta t),t_k)\right\}. \tag{4.8}$$

The first term in the right-hand side of (4.7) can be estimated by (4.8) and the weak convergence assumption (2.2) as

$$\frac{1}{\Delta t}\left| v(x_j,t_{k+1}) - \sum_{i=1}^{s} w_i\{\bar\gamma(x_j,\Delta_i) + v(\bar y(x_j,\Delta_i),t_k)\}\right| \le C\Delta t^p \tag{4.9}$$

(note that we are working on a single time step and that v is supposed to be smooth). Using (3.9), the second term may be estimated as

$$\begin{aligned}
&\frac{1}{\Delta t}\left|\sum_{i=1}^{s} w_i\{\bar\gamma(x_j,\Delta_i)+v(\bar y(x_j,\Delta_i),t_k)\}-\sum_{i=1}^{s} w_i\{\bar\gamma(x_j,\Delta_i)+I[V(t_k)](\bar y(x_j,\Delta_i))\}\right| \\
\le&\frac{1}{\Delta t}\sum_{i=1}^{s} w_i|v(\bar y(x_j,\Delta_i),t_k)\}-I[V(t_k)](\bar y(x_j,\Delta_i))| \\
\le&\frac{1}{\Delta t}\sum_{i=1}^{s} w_i C\Delta x^r = C\frac{\Delta x^r}{\Delta t}, \qquad (4.10)
\end{aligned}$$

which, put together with (4.9) and accumulated over all components, proves (4.6). □

Remark 4.2. A different interpretation of the consistency of the scheme can also be given with no use of stochastic arguments. Consider the difference operator obtained by neglecting the interpolation phase in the weighted sum on the right-hand side of (3.8), in the simplest case given by (2.3), and in one space dimension with $g\equiv 0$. By a Taylor expansion, and collecting all higher order terms in some $\mathcal{O}(\Delta t^2)$, we have

$$\begin{aligned}
&v\left(x_j+a\Delta t\pm\sqrt{2\nu\Delta t}\right) \\
=&v(x_j)+\left(a\Delta t\pm\sqrt{2\nu\Delta t}\right)v_x(x_j)+\frac{1}{2!}\left(a\Delta t\pm\sqrt{2\nu\Delta t}\right)^2 v_{xx}(x_j) \\
&+\frac{1}{3!}\left(a\Delta t\pm\sqrt{2\nu\Delta t}\right)^3 v_{xxx}(x_j)+\mathcal{O}(\Delta t^2) \\
=&v(x_j)+\left(a\Delta t\pm\sqrt{2\nu\Delta t}\right)v_x(x_j)+\frac{1}{2!}\left(2\nu\Delta t\pm 2a\Delta t\sqrt{2\nu\Delta t}\right)v_{xx}(x_j) \\
&+\frac{1}{3!}\left(\pm\sqrt{2\nu\Delta t}^3\right)v_{xxx}(x_j)+\mathcal{O}(\Delta t^2),
\end{aligned}$$

so that

$$\begin{aligned}
&\frac{1}{2}\left[v\left(x_j+a\Delta t+\sqrt{2\nu\Delta t}\right)+v\left(x_j+a\Delta t-\sqrt{2\nu\Delta t}\right)\right] \\
=&v(x_j)+\Delta t\left[a\,v_x(x_j)+\nu v_{xx}(x_j)\right]+\mathcal{O}(\Delta t^2).
\end{aligned}$$

Note that, in the right-hand side, the term in square brackets is precisely the evolution operator computed at x_j.

4.3 Convergence rate

We finally sum up the analysis performed so far in a convergence theorem.

Theorem 4.3. *Let the family of schemes* (4.2) *satisfy* (4.3) (*in particular, in the cases stated in Remark* 4.1). *Then, for any* $k\in[1,T/\Delta t]$,

$$\left\|V^k-V(t_k)\right\|_\alpha\to 0 \tag{4.11}$$

for $\Delta t\to 0$, $\Delta x=o\left(\Delta t^{1/r}\right)$. *If, in addition,* (2.2) *holds with order* p *and, for any* $t\in[0,T]$, $v(\cdot,t)\in C^r(\mathbb{R}^N)$, *then*

$$\left\|V^k-V(t_k)\right\|_\alpha\le C\left(\Delta t^p+\frac{\Delta x^r}{\Delta t}\right). \tag{4.12}$$

Remark 4.3. Note that the convergence estimate requires the regularity of the solution, but *not* the uniform parabolicity of the equation, since both the representation formula (1.5) and the weak discretization of SDEs are suitable for the degenerate case.

Remark 4.4. The condition $\Delta x=o(\Delta t^{1/r})$ is required in order for the estimate (4.6) to vanish. The scheme is therefore unconditionally stable, but conditionally consistent. Moreover, (4.6) shows a nontrivial interplay between the two discretization steps (see [10] for an in-depth discussion of this point); the order of consistency of the scheme is maximized by setting

$$\Delta t\sim\Delta x^{\frac{r}{p+1}}, \tag{4.13}$$

and with this choice the theoretical convergence rate of the scheme is $\frac{rp}{p+1}$ (with respect to the only independent discretization step Δx).

In practice, if both space and time discretizations are of the same order (e.g., $\mathbb{P}_1$ in space and Euler in time), (4.13) results in a conventional hyperbolic-type CFL condition. If the order of time discretization is higher, consistency rate would be maximized with $\Delta t=o(\Delta x)$, although, in practical implementations, higher order space reconstructions are rather used as a tool to reduce undesired numerical dissipation, and no optimization of the rate is performed. In the opposite situation (time discretization of higher order), consistency rate is maximized under an inverse CFL condition $\Delta x=o(\Delta t)$. The only discretization of interest in this case, e.g. $\mathbb{P}_1$ in space, Heun or Crank-Nicolson in time, will be considered in the numerical test section, since it combines monotonicity with a theoretical consistency rate beyond the unity.

4.4 Fourier analysis of the scheme

A different insight into the mechanism of the scheme may be given by directly proving convergence with Fourier analysis tools. We consider therefore the behaviour of the scheme on a one-dimensional, homogeneous, constant coefficient equation, that is

$$\begin{cases} v_t=\nu v_{xx}+av_x, & x\in\mathbb{R},\\ v(x,0)=v_0(x), \end{cases} \tag{4.14}$$

whose exact solution is given by the convolution

$$v(x,t)=\frac{e^{-\frac{(x+at)^2}{4\nu t}}}{\sqrt{4\pi\nu t}}*v_0(x). \tag{4.15}$$

According to (3.10), the fully discrete approximation of (4.14) reads

$$V^{k+1}=\Psi V^k=\sum_{i=1}^{s}w_i\Psi^{(i)}V^k, \tag{4.16}$$

where the banded infinite matrices $\Psi^{(i)}$ correspond to the matrices used in approximating the advection equations

$$\begin{cases} u_t=\left(a+\frac{\sqrt{2\nu}\Delta_i}{\Delta t}\right)u_x, \quad x\in\mathbb{R}, \\ u(x,0)=u_0(x). \end{cases} \tag{4.17}$$

In this setting, $\Psi^{(i)}=\left(\psi_{jl}^{(i)}\right)$, so that

$$I[V^k](x_j+a\Delta t+\sqrt{2\nu}\Delta_i))=\sum_l \psi_{jl}^{(i)}v_l^k, \tag{4.18}$$

with $x_j=j\Delta x$ and the condition $\psi_{jl}^{(i)}=\psi_{j+1,l+1}^{(i)}$. This condition requires both linearity and translation invariance of the reconstruction operator $I[\cdot]$, and in practice typically corresponds to the case of Lagrange interpolation (usually, the stencil is symmetric and therefore the degree of the interpolating polynomial is odd). In this situation (see [11]) the reconstruction can be set in the form

$$I[U](x)=\sum_l u_l\phi\left(\frac{x-x_l}{\Delta x}\right) \tag{4.19}$$

for a suitable reference basis function ϕ, piecewise polynomial of degree $m=r-1\geq 1$.

Carrying out the transformations in the Fourier domain, we obtain from (4.15):

$$\hat{v}(\omega,t)=\mathcal{F}[v](\omega,t)=e^{iat\omega-\nu t\omega^2}\hat{v}_0(\omega). \tag{4.20}$$

where i denotes the imaginary unit. On the other hand, we get from (4.16)

$$\hat{V}^{k+1}(\omega)=\hat{\Psi}(\omega)\hat{V}^k(\omega) \tag{4.21}$$

and hence

$$\hat{V}^k(\omega)=\hat{\Psi}(\omega)^k\hat{V}^0(\omega), \tag{4.22}$$

where the (infinite) matrix product in the right-hand side of (4.16) is understood as a discrete convolution, and the Fourier transform of a sequence as the transformation of its

pulsed continuous equivalent, more precisely:

$$\hat{V}^k(\omega)=\mathcal{F}\left[\sum_j v_j^k\delta(x-x_j)\right](\omega),$$
$$\hat{\Psi}(\omega)=\mathcal{F}\left[\sum_j \psi_{0j}\delta(x-x_j)\right](\omega).$$

By (4.19), it is clear that the reconstructed numerical solution $I[V^k]$ amounts to a convolution of the sequence V^k with the scaled basis function $\tilde{\phi}(x)=\phi(x/\Delta x)$. Turning to the Fourier domain, this gives

$$\mathcal{F}\left[I[V^0]\right](\omega)=\hat{V}^0(\omega)\mathcal{F}[\tilde{\phi}](\omega), \tag{4.23}$$
$$\mathcal{F}\left[I[V^k]\right](\omega)=\hat{V}^k(\omega)\mathcal{F}[\tilde{\phi}](\omega), \tag{4.24}$$

so that, using also (4.22):

$$\mathcal{F}\left[I[V^k]\right](\omega)=\hat{\Psi}(\omega)^k\hat{V}^0(\omega)\mathcal{F}[\tilde{\phi}](\omega)=\hat{\Psi}(\omega)^k\mathcal{F}\left[I[V^0]\right](\omega). \tag{4.25}$$

Since (under reasonable smoothness assumptions) $\mathcal{F}\left[I[V^0]\right](\omega)\to\hat{v}_0(\omega)$ as $\Delta x\to 0$, this proves that $\mathcal{F}\left[I[V^k]\right](\omega)\to\hat{v}(\omega,t)$ as soon as $\hat{\Psi}(\omega)^k\to e^{iat\omega-\nu t\omega^2}$.

Recovering the asymptotic behaviour of $(\hat{\Psi})^k$ is a well-known problem in probability theory, and the answer is given by the central limit theorem as far as the sequence ψ_{0l} is made of positive elements. This condition fails in general in our case, but we will follow similar steps.

Step 1. As a start, we show that $|\hat{\Psi}(\omega)|\leq 1$. In fact, this is equivalent to the Von Neumann condition of L^2 stability. Recalling (4.3), we have

$$|\hat{\Psi}(\omega)|\leq\sum_{i=1}^{s} w_i|\hat{\Psi}^{(i)}(\omega)|\leq 1. \tag{4.26}$$

The last inequality in (4.26) follows from the L^2 stability of the schemes which approximate equation (4.17) for any Δ_i, this being proved in [8], [1]. We remark that (4.26) implies that $\hat{\Psi}(\omega)^k\leq 1$ for any $k\geq 0$.

Step 2. Let us compute the Taylor series of $\hat{\Psi}(\omega)$ centered in $\omega=0$. By known properties of the Fourier transform, the required derivatives can be computed starting from the moments of the sequence ψ_{0l}, so that

$$\hat{\Psi}(0)=\sum_l \psi_{0l}=\sum_{i=1}^{s} w_i\sum_l \psi_{0l}^{(i)}=1, \tag{4.27}$$

which follows from the fact that the reconstruction is exact on constant functions. On the other hand,

$$\begin{aligned}\hat{\Psi}'(0) &= -\boldsymbol{i}\sum_l x_l\psi_{0l} = -\boldsymbol{i}\sum_{i=1}^{s} w_i \sum_l x_l \psi_{0l}^{(i)} \\ &= -\boldsymbol{i}\sum_{i=1}^{s} w_i(a\Delta t+\sqrt{2\nu}\Delta_i) = -\boldsymbol{i}a\Delta t - \boldsymbol{i}\sqrt{2\nu}\sum_{i=1}^{s} w_i\Delta_i = -\boldsymbol{i}a\Delta t. \end{aligned} \tag{4.28}$$

In (4.28), we have used both the fact that $\sum_l x_l\psi_{0l}^{(i)}$ is nothing but the reconstruction (which has been supposed to be exact) of the linear function x in the point $x=a\Delta t+\sqrt{2\nu}\Delta_i$, and the condition (3.6). From the second moment we have

$$\begin{aligned}\hat{\Psi}''(0) &= -\sum_l x_l^2\psi_{0l} = -\sum_{i=1}^{s} w_i \sum_l x_l^2 \psi_{0l}^{(i)} = -\sum_{i=1}^{s} w_i(a\Delta t+\sqrt{2\nu}\Delta_i)^2 \\ &= -a^2\Delta t^2 - 2\nu\sum_{i=1}^{s} w_i\Delta_i^2 + \mathcal{O}(\Delta x^r) \end{aligned} \tag{4.29}$$

in which we have used again the facts that $\sum_l x_l^2\psi_{0l}$ is the reconstruction of the function x^2 at the point $x=a\Delta t+\sqrt{2\nu}\Delta_i$, that this reconstruction is performed with a worst-case error of $\mathcal{O}(\Delta x^r)$ (in fact, this error vanishes if $m\geq 2$) and that (3.6) holds. Using (3.7) and the consistency condition $\Delta x^r = o(\Delta t)$, we obtain at last

$$\hat{\Psi}''(0) = -2\nu\Delta t + o(\Delta t). \tag{4.30}$$

It is easy to show by means of the same arguments that, since $a\Delta t+\sqrt{2\nu}\Delta_i = \mathcal{O}(\sqrt{\Delta t})$, successive derivatives satisfy

$$\hat{\Psi}^{(n)}(0) = (-\boldsymbol{i})^n \sum_{i=1}^{s} w_i(a\Delta t+\sqrt{2\nu}\Delta_i)^n + \mathcal{O}(\Delta x^r) = \mathcal{O}(\Delta t^{n/2}) + \mathcal{O}(\Delta x^r), \tag{4.31}$$

and, by the condition $\Delta x^r = o(\Delta t)$, that $\hat{\Psi}^{(n)}(0) = o(\Delta t)$ as soon as $n>2$. We obtain therefore:

$$\hat{\Psi}(\omega) = 1 + \Delta t(a\boldsymbol{i}\omega - \nu\omega^2) + o(\Delta t). \tag{4.32}$$

Step 3. Setting now $k = t/\Delta t$ and letting $\Delta t \to 0$:

$$\hat{\Psi}(\omega)^{\frac{t}{\Delta t}} \to e^{\boldsymbol{i}at\omega - \nu t\omega^2}, \tag{4.33}$$

which states the convergence (in terms of Fourier transforms) of the approximate evolution operator in (4.22) to the exact one. This finally shows that $\mathcal{F}\left[I[V^k]\right](\omega) \to \hat{v}(\omega,t)$.

Remark 4.5. We stress that the gaussian term in the Fourier transform (and hence, the possibility of treating the second-order derivative) comes from the presence of a nonzero centered second moment in the sequence ψ_{0l}.

Remark 4.6. Although convergence of Fourier transforms would in principle imply only *weak* convergence of numerical solutions, in practice we expect that due to even minimal smoothness assumptions, numerical solutions would converge in a stronger topology. This is not necessarily true for the evolution operator, in the sense that $\mathcal{F}^{-1}\left[\hat{\Psi}^k\right](x)$ may not converge (in a strong topology) to the kernel appearing in the convolution (4.15). This point has a remarkable influence on the accuracy of the approximation and will be further discussed in the next section.

5 Numerical domain of dependence

While under the parabolic CFL condition $\Delta t = O(\Delta x^2)$, or in case of strongly advection-dominated problems, the "upwind" points $x_j \pm c\sqrt{\nu \Delta t}$ can be adjacent to x_j, with a stronger diffusion or a less restrictive $\Delta t/\Delta x$ relationship they will fall in a "far" cell of the grid, and in practice this can lead to an unsatisfactory behaviour of the scheme, if no special care is taken. In order to analyse in greater detail the behaviour of the scheme for equations with a relevant diffusion term, we consider the heat equation

$$\begin{cases} v_t = \frac{1}{2} v_{xx}, \\ v_0(x) = \begin{cases} 1, & \text{if } -0.5 \le x \le 0.5, \\ 0, & \text{else,} \end{cases} \end{cases} \tag{5.1}$$

with $\Omega = (-1,1)$, $v(-1,t) = v(1,t) = 0$.

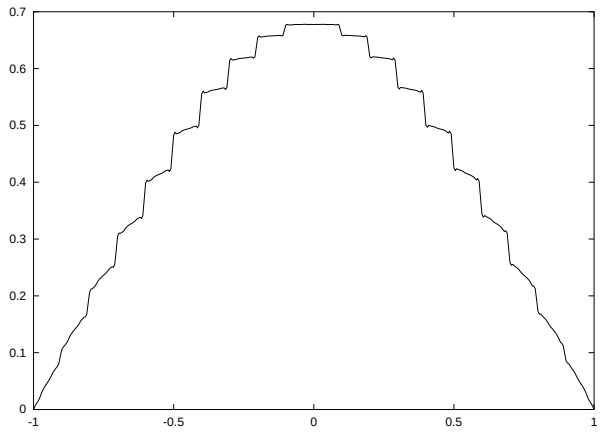

Figure 1: Approximate solution for problem (5.1), $\Delta t = \Delta x = 0.01$.

Fig. 1 shows the approximate solution at $t = 1$ with an Euler/cubic discretization for $\Delta t = 0.01$ (i.e., with 100 time steps), on a space grid of 201 nodes. The highly irregular behaviour of the scheme can be explained by a more in-depth analysis. With the parameters chosen, the two "upwind" points for the node x_j are $x_j \pm \sqrt{2\nu \Delta t} = x_{j\pm 10}$, which are the

numerical domain of dependence at the previous time step. Going backwards one more time step, the numerical domain of dependence is made by the points x_j, x_{j-20} and x_{j+20}, and so forth. The resulting "discrete Green function", associated to the initial condition

$$v_0(x_j) = e_0 = \begin{cases} 1, & \text{if } j=0, \\ 0, & \text{else,} \end{cases}$$

is shown in the uppermost row of Fig. 2, with respectively $\mathbb{P}_1$ and cubic interpolation.

It is apparent that the domain of dependence develops "holes" which cause the oscillations seen in Fig. 1. However, the situation in which the upwind points precisely coincide with other grid nodes is unlikely. In a more realistic setting, the numerical domain of dependence would also include (in a $\mathbb{P}_1$ reconstruction) one node left and one node right of the point $x_j \pm \sqrt{2\nu\Delta t}$. Therefore, a "hole" of width $2\sqrt{2\nu\Delta t}$ could be filled up in a number of steps

$$k = \frac{2\sqrt{2\nu\Delta t}}{2\Delta x}$$

so that keeping fixed the final time T, the condition $T \geq k\Delta t$ (which would be necessary to avoid such "holes" in the numerical domain of dependence) yields

$$\Delta t \leq \frac{T^{2/3}\Delta x^{2/3}}{(2\nu)^{1/3}}. \tag{5.2}$$

In practice, it would be reasonable to require the stronger condition

$$\Delta t \ll \frac{T^{2/3}\Delta x^{2/3}}{(2\nu)^{1/3}} \tag{5.3}$$

in order to obtain a more regular dependence. Although this condition has been obtained for the Euler/$\mathbb{P}_1$ coupling, a similar analysis in other cases would coincide up to a constant factor (with magnitude close to the unity) on the right-hand side. Neglecting such constant, we obtain the condition

$$\lambda \equiv \frac{\nu^{1/3}\Delta t}{T^{2/3}\Delta x^{2/3}} \ll 1. \tag{5.4}$$

In the first two plots of Fig. 2, $\lambda \approx 0.17$. In the other plots, discrete Green functions are shown for different values of Δt, and accordingly of λ. In the second row $\Delta t = 0.005$ (200 time steps) and $\lambda \approx 0.085$. In the third row $\Delta t = 0.00333$ (300 time steps) and $\lambda \approx 0.057$ whereas in the last row $\Delta t = 0.0025$ (400 time steps) and $\lambda \approx 0.043$. Left plots refer to solutions computed with a $\mathbb{P}_1$ interpolation, right plots to solution computed with cubic interpolation. It is apparent that the regularization of the numerical domain of dependence is faster in the monotone case, and higher order interpolation may require lower values of λ.

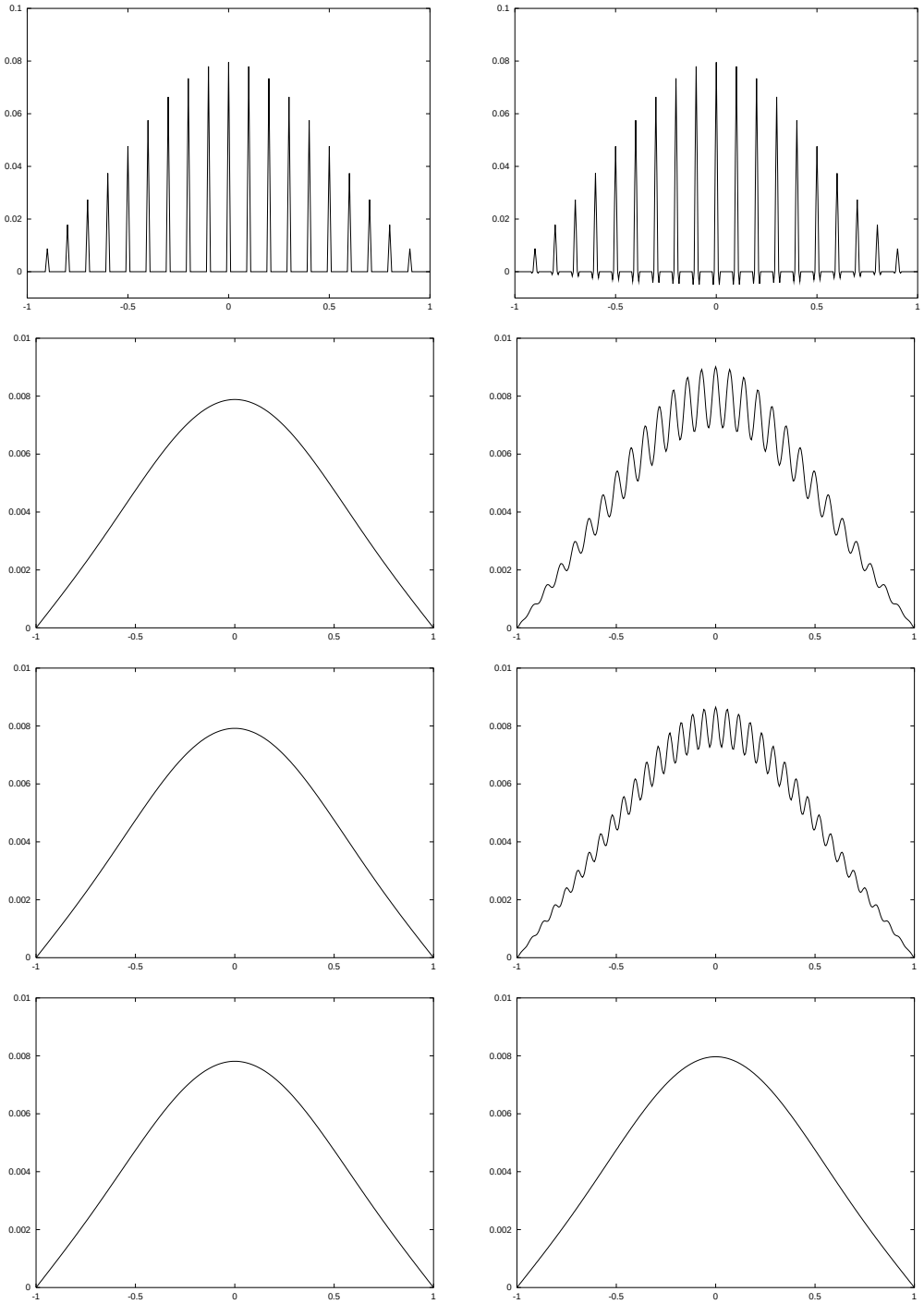

Figure 2: Discrete Green functions for problem (5.1), Δx=0.01, λ=0.17 (uppermost line) to λ=0.043 (lowermost line), with $\mathbb{P}_1$ (left) and cubic (right) reconstruction.

It is interesting to note that condition (5.4) is easier to satisfy with strongly advection-dominated problems (ν small) or in the large-time simulation (T large). In the limit, this condition is always satisfied when the stationary solution is computed ($T=\infty$), as in [2].

The relationship $\Delta t=\mathcal{O}(\Delta x^{2/3}/\nu^{1/3})$ allows to work at constant or slightly increasing Courant numbers in refining the grid, this being a significant improvement over the usual parabolic CFL condition $\Delta t=\mathcal{O}(\Delta x^2/\nu)$ of explicit Eulerian schemes. Moreover, relating the time step to the cubic root of $\Delta x^2/\nu$, it also allows for a less critical choice of the time step, for example in case of local refinements.

6 Numerical tests

This section gives some numerical example showing the behaviour of the scheme on test cases in $\mathbb{R}^1$ and $\mathbb{R}^2$. Examples in $\mathbb{R}^1$ will present a detailed analysis of the convergence history for various couplings of SDE scheme and reconstruction. In the $\mathbb{R}^2$ examples we will focus instead on a degenerate equation, examining respectively the smooth and the nonsmooth case.

6.1 Tests in $\mathbb{R}^1$

We start with a couple of simple one-dimensional test intended to illustrate and check in greater detail the previous convergence results. Computations for both Examples 6.1 and 6.2 have been carried out for the Euler/$\mathbb{P}_1$, Heun/$\mathbb{P}_2$, Heun/$\mathbb{P}_1$and Heun/cubic coupling on successive grids of 21, 51, 101, 201, 501 and 1001 nodes; errors are computed in the discrete L^1 norm due to the possibility of peaks or boundary layers in the solution. For the first two choices, (4.13) results in choosing a constant Courant number along the refinement. In the third case, consistency rate is maximized under an inverse CFL condition, whereas in the fourth, (4.13) requires the Courant number to vanish along the refinement.

We have set the viscosity to $\nu=10^{-n}$ (for $n=0,\cdots,3$), so that the tests range from being diffusion-dominated to advection-dominated. In all cases, the relationship between Δt and Δx has been chosen in order to have $\lambda\lesssim 0.05$ on the coarsest space-time grid. In particular, refinements at constant Courant number have been implemented with the conditions

$$\begin{cases}\Delta t=\Delta x/5, & \text{if } \nu=1,\\ \Delta t=\Delta x/2, & \text{if } \nu=0.1,\\ \Delta t=\Delta x, & \text{if } \nu=0.01,\\ \Delta t=2\Delta x, & \text{if } \nu=0.001.\end{cases}$$

Refinements for the Heun/$\mathbb{P}_1$ scheme have been implemented with $\Delta t\approx 0.13\cdot\nu^{-1/3}\Delta x^{2/3}$ and for the Heun/cubic scheme with $\Delta t\approx 0.13\cdot\nu^{-1/3}\Delta x^{4/3}$.

In order to obtain the convergence rate of the scheme, we use a reference solution computed by the Heun/$\mathbb{P}_2$ scheme with 10001 nodes. Tables 3 and 4 show the convergence rates computed between the extreme values of Δx. Because of the various refinement strategies, and in order to compare the efficiency of schemes, numbers in brackets also report convergence rates with respect to the computational complexity, this being measured as the number of points in the space-time grid.

Finally, Dirichlet boundary conditions have been treated following [8].

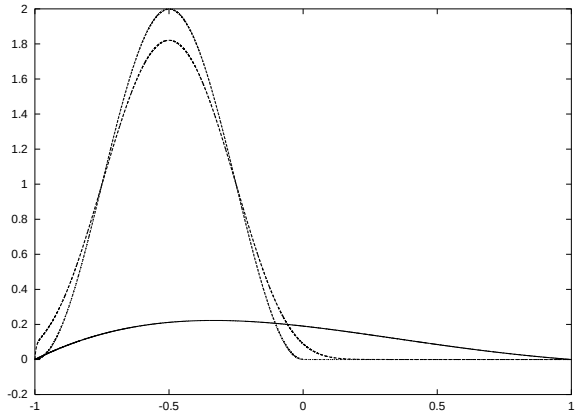

Figure 3: Reference solutions for Example 6.1.

Example 6.1. We first consider the equation

$$\begin{cases} v_t = \nu v_{xx} + v_x, \\ v_0(x) = \begin{cases} 1-\cos(2\pi x), & \text{if } x \geq 0, \\ 0, & \text{else,} \end{cases} \end{cases}$$

posed in $\Omega=(-1,1)$, with boundary conditions $v(-1,t)=v(1,t)=0$. The approximations are computed at $T=1$. In this equation, characteristics advect the initial condition to the left at constant speed. In the inviscid case, the solution would remain of C^1 with support in $(-1,1)$, but in fact diffusion may cause a small layer at the outflow boundary (that is, at $x=-1$). Fig. 3 shows the reference numerical solutions, whereas Table 3 compares

Table 3: Overall convergence rates, Example 6.1.

scheme	$\nu=1$		$\nu=0.1$		$\nu=0.01$		$\nu=0.001$	
Euler/$\mathbb{P}_1$	1.02	(0.51)	1.15	(0.58)	0.53	(0.27)	0.49	(0.25)
Heun/$\mathbb{P}_1$	0.89	(0.53)	1.30	(0.78)	1.23	(0.74)	1.81	(1.09)
Heun/$\mathbb{P}_2$	1.73	(0.87)	2.06	(1.03)	2.31	(1.16)	2.45	(1.23)
Heun/cubic	2.34	(1.0)	2.33	(1.0)	2.33	(1.0)	2.11	(1.09)

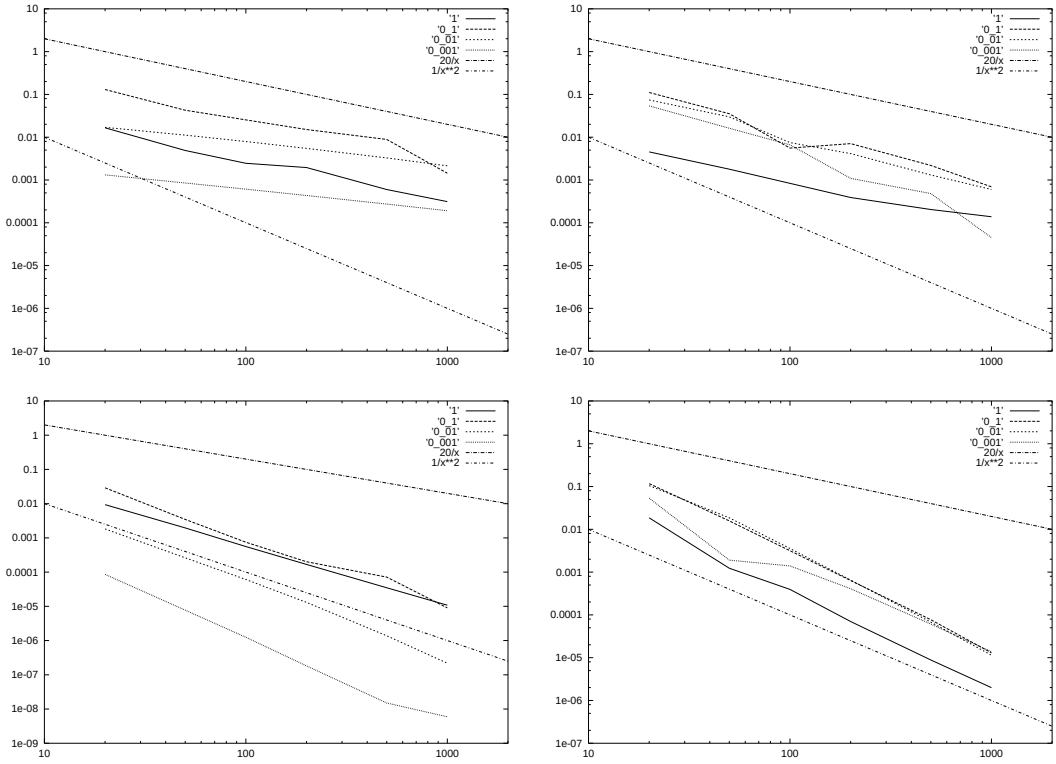

Figure 4: Convergence of Euler/$\mathbb{P}_1$ (upper left), Heun/$\mathbb{P}_1$ (upper right), Heun/$\mathbb{P}_2$ (lower left) schemes, Heun/cubic (lower right), Example 6.1.

the schemes in terms of convergence rates. Lastly, Fig. 4 shows numerical errors versus number of nodes with the reference slopes of a first- and a second-order convergence.

Example 6.2. We next consider the nonconstant coefficient equation

$$\begin{cases} v_t = \nu v_{xx} + x v_x + 1, \\ v_0(x) = x, \end{cases}$$

posed in $\Omega=(-1,1)$, with boundary conditions $v(-1,t)=-1$, $v(1,t)=1$. The approximations are computed at $T=4$. In this equation, characteristics point towards the origin, and

Table 4: Overall convergence rates, Example 6.2.

scheme	$\nu=1$		$\nu=0.1$		$\nu=0.01$		$\nu=0.001$	
Euler/$\mathbb{P}_1$	1.43	(0.72)	0.79	(0.4)	0.71	(0.36)	0.86	(0.43)
Heun/$\mathbb{P}_1$	0.41	(0.25)	1.4	(0.84)	0.98	(0.59)	0.92	(0.54)
Heun/$\mathbb{P}_2$	1.04	(0.52)	1.47	(0.74)	1.99	(1.0)	1.50	(0.75)
Heun/cubic	1.4	(0.6)	2.09	(0.9)	1.59	(0.68)	1.52	(0.65)

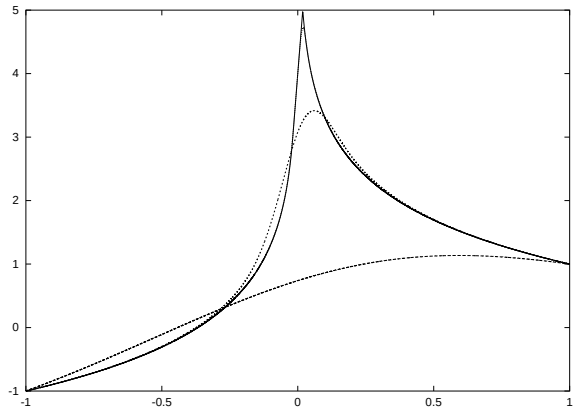

Figure 5: Reference solutions for Example 6.2.

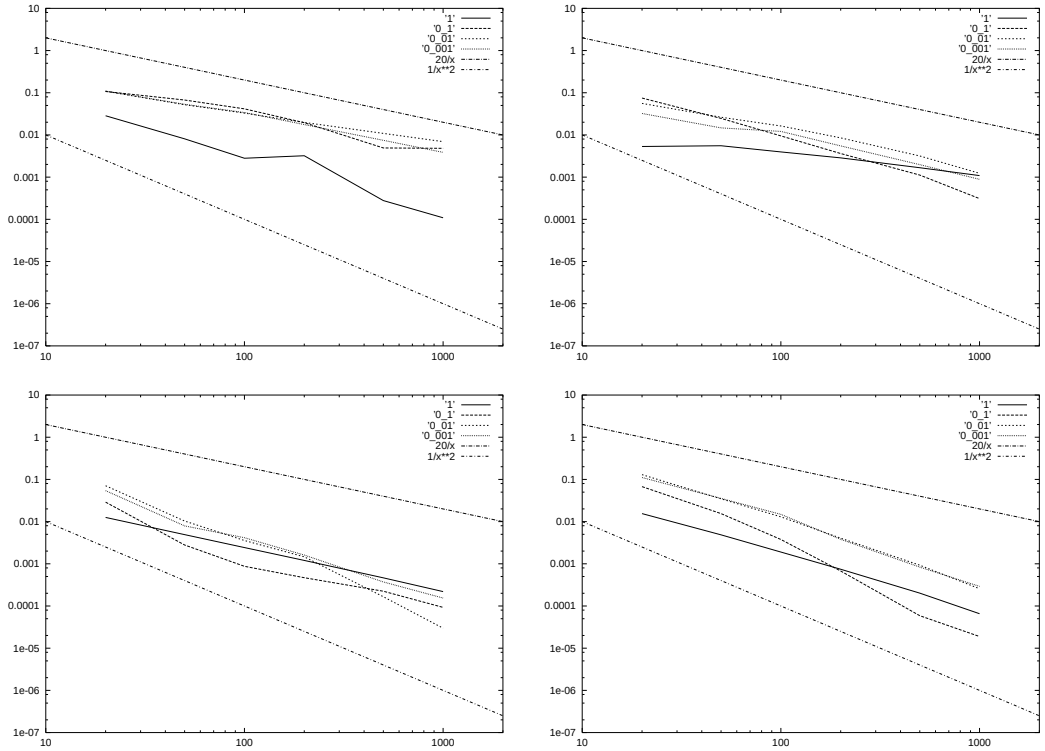

Figure 6: Convergence of Euler/$\mathbb{P}_1$ (upper left), Heun/$\mathbb{P}_1$ (upper right), Heun/$\mathbb{P}_2$ (lower left) schemes, Heun/cubic (lower right), Example 6.2.

in the inviscid case two singularities of u_x are associated to the points $\pm e^{-t}$. The source term tends to cause a sharp peak at the rightmost of these points. Again, Fig. 5 shows the reference solutions, Table 4 a comparison of convergence rates and Fig. 6 numerical errors versus number of nodes.

Although the measured convergence rates may fluctuate around the predicted ones, the advantage in using higher order schemes is apparent from the comparison with the Euler/$\mathbb{P}_1$ scheme. This advantage is better seen in Example 6.1, which corresponds to a smoother situation. Both examples confirm, however, that situation gets more complex in the case of diffusion-dominated problems, in which it seems that performances of the scheme may be increased either by monotonicity of the reconstruction (see Fig. 2) or by very small Courant numbers like those used in the Heun/cubic refinement. We think that a convincing analysis of the diffusion-dominated case would surely need further investigations.

At the efficiency level, note that $\mathbb{P}_2$ reconstruction might be now and then preferred to cubic because of the lesser number of time steps. However, as observed in Remark 4.4, the usual practice when very high-order space reconstructions are used is not to optimize the consistency rate, but rather to use large, constant Courant numbers (this reduces numerical dispersion while keeping computational complexity lower).

6.2 Tests in $\mathbb{R}^2$

We perform here two tests in two space dimensions. In both cases, we consider Eq. (1.1) in $\mathbb{R}^2$ with constant advection speed and degenerate diffusion, in particular

$$A=\begin{pmatrix} \frac{1}{64} & \frac{\sqrt{3}}{64} \\ \frac{\sqrt{3}}{64} & \frac{3}{64} \end{pmatrix}, \qquad f\equiv\begin{pmatrix} -1 \\ -3 \end{pmatrix}, \qquad g\equiv 0$$

posed in $\Omega=(-2,2)^2$, with biperiodic boundary conditions. The equation is slightly advection-dominated, and diffusion is degenerate along a direction rotated by 30° with respect to the grid geometry. In this test, diffusion and advection are not aligned one another, and neither of the two is oriented along relevant directions of the space grid. The approximate solutions are compared at $T=4$ (that is, at the time at which a rigid advection with the same speed would bring back the solution to its original configuration).

Example 6.3. In the first example, we test the convergence of schemes on a smooth solution. The initial condition is

$$v_0(x)=\sin\left(\frac{\pi}{2}x_1\right)\sin\left(\frac{\pi}{2}x_2\right).$$

The exact solution can be computed by decoupling advection and diffusion, and at $t=4$ its expression (in single precision) is

$$v(x,4)=0.6184912\cdot\sin\left(\frac{\pi}{2}x_1\right)\sin\left(\frac{\pi}{2}x_2\right)+0.3021893\cdot\cos\left(\frac{\pi}{2}x_1\right)\cos\left(\frac{\pi}{2}x_2\right).$$

Here, we have implemented a more conventional strategy of refinement, by working at constant Courant number, with $\Delta t=1.25\cdot\Delta x$ ($\Delta t=0.1$ on a 51×51 grid). The schemes

Table 5: Errors and overall convergence rates, Example 6.3.

nodes	Heun/$\mathbb{P}_1$	Heun/$\mathbb{P}_2$	Heun/cubic
26	1.056	$2.182\cdot10^{-2}$	$1.059\cdot10^{-2}$
51	0.529	$6.836\cdot10^{-3}$	$1.419\cdot10^{-3}$
101	0.27	$1.437\cdot10^{-3}$	$1.86\cdot10^{-4}$
rate	0.98	1.96	2.92

tested are obtained coupling the Heun scheme with $\mathbb{P}_1$, $\mathbb{P}_2$ and cubic reconstructions (this would theoretically result in a first-order and two second-order schemes).

In this example, solution is smooth despite degeneracy of the operator, and numerical schemes behave according to the theory (Heun/$\mathbb{P}_1$ and Heun/$\mathbb{P}_2$) or even better (Heun/cubic). Errors and global convergence rates are reported in Table 5, whereas Fig. 7 shows initial condition and numerical solution at $t=4$.

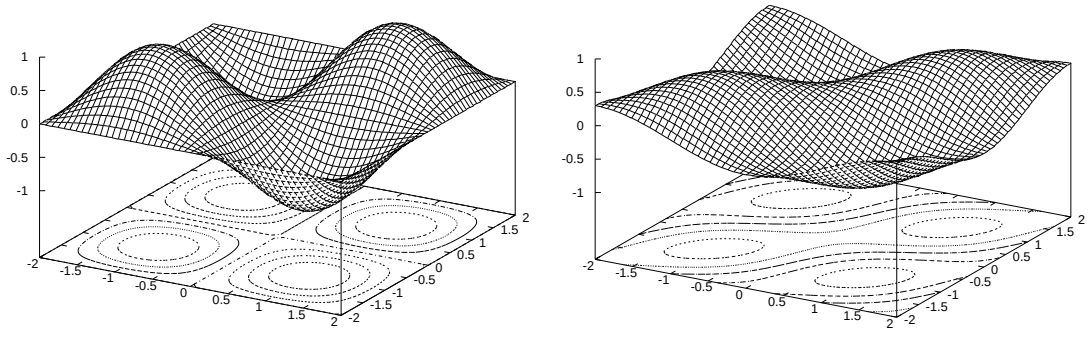

Figure 7: Initial condition (left) and Heun/cubic solution (right), Example 6.3.

Example 6.4. In this second example, the initial condition is the characteristic function of a unit square, rotated by 30°, so that the solution is diffused along one of the axes of the square, whereas it remains discontinuous along the other. Fig. 8 shows the initial condition (upper left) and the numerical solutions obtained by coupling the Heun scheme with different space reconstructions, at $T=4$, on a grid of 51×51 nodes, with $\Delta t=0.1$. While the $\mathbb{P}_1$ scheme is clearly too viscous, cubic reconstruction (lower left) has a better resolution of the discontinuity (within about 3-4 mesh sizes), although it also introduces some over- and undershoot in the computation. Such oscillations are avoided by the third-order ENO scheme (lower right) at the price of a higher complexity.

References

[1] N. Besse and M. Mehrenberger, Convergence of classes of high-order semi-Lagrangian schemes for the Vlasov-Poisson system, Math. Comp., 77 (2008), 93–123.

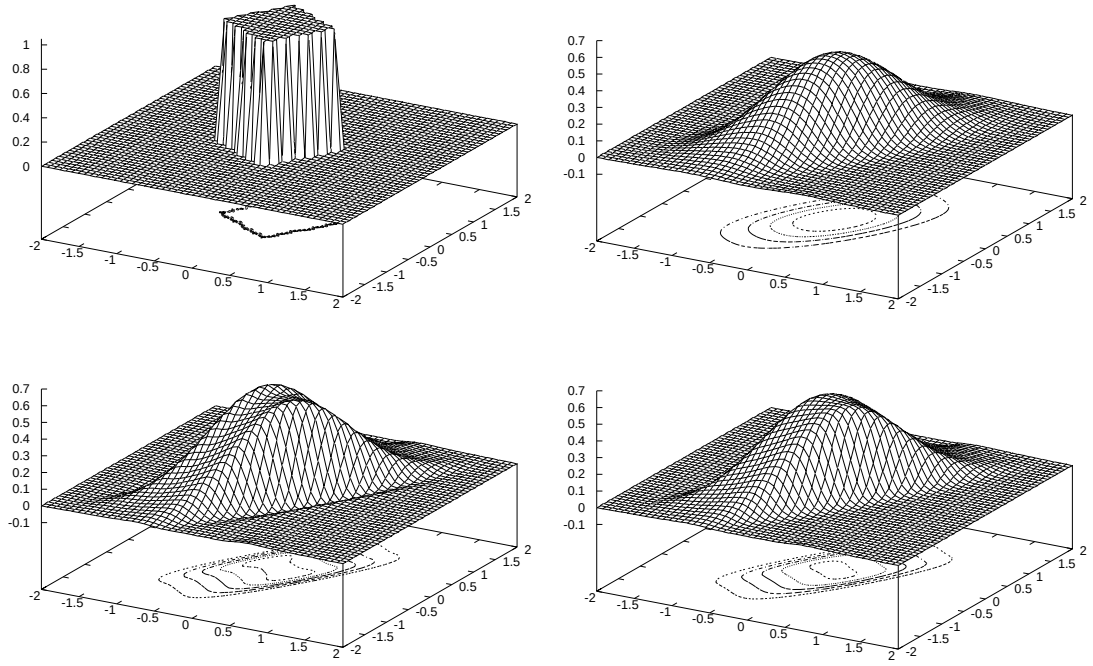

Figure 8: Initial condition (upper left), Heun/$\mathbb{P}_1$ solution (upper right), Heun/cubic solution (lower left), Heun/ENO3 solution (lower right), Example 6.4.

[2] F. Camilli and M. Falcone, An approximation scheme for the optimal control of diffusion processes, RAIRO Model. Math. Anal. Numer., 29 (1995), 97–122.

[3] E. Carlini, M. Falcone and R. Ferretti, A semi-Lagrangian scheme for the curve shortening flow in codimension-2, J. Comput. Phys., 225 (2007), 1388–1408.

[4] C.Z. Cheng and G. Knorr, The integration of the Vlasov equation in configuration space, J. Comput. Phys., 22 (1976), 330–351.

[5] R. Courant, E. Isaacson and M. Rees, On the solution of nonlinear hyperbolic differential equations by finite differences, Comm. Pure Appl. Math., 5 (1952), 243-255.

[6] M.G. Crandall, H. Ishii and P.L. Lions, User's guide to viscosity solutions of second order partial differential equations, Bull. Amer. Math. Soc., 27 (1992), 1–67.

[7] J. Douglas Jr. and T. F. Russell, Numerical methods for convection-dominated diffusion problems based on combining the method of characteristics with finite element or finite difference procedures, SIAM J. Num. Anal., 19 (1982), 871-885.

[8] M. Falcone and R. Ferretti, Convergence analysis for a class of semi-Lagrangian advection schemes, SIAM J. Num. Anal., 35 (1998), 909–940.

[9] M. Falcone, R. Ferretti, Consistency of a large time-step scheme for mean curvature motion, in F. Brezzi, A. Buffa, S. Corsaro and A. Murli (eds), "Numerical Mathematics and Advanced Applications – ENUMATH 2001", Springer-Verlag, Berlin, 2003.

[10] M. Falcone, R. Ferretti e T. Manfroni, Optimal discretization steps for a class of semi-Lagrangian schemes, in "Numerical methods for viscosity solutions and applications (Heraklion, 1999)", Ser. Adv. Math. Appl. Sci. 59, World Sci. Publishing, River Edge, NJ, 2001.

[11] R. Ferretti, Equivalence of semi-Lagrangian and Lagrange-Galerkin schemes under constant advection speed, submitted.
[12] R. Ferretti, On the relationship between semi-Lagrangian and Lagrange-Galerkin schemes, in preparation.
[13] R. Ferretti e G. Perrone, On the stability of semi-Lagrangian advection schemes under finite element interpolation, in "Applied and industrial mathematics in Italy II", 339–350, Ser. Adv. Math. Appl. Sci., 75, World Sci. Publishing, Singapore, 2007
[14] A. Ghizzo, P. Bertrand, M.M. Shoucri, T. W. Johnston, E. Fijalkow and M.R. Feix, A Vlasov code for the numerical simulation of stimulated Raman scattering, J. Comput. Phys., 90 (1990), 431–457.
[15] P.E. Kloeden and E. Platen, Numerical solution of stochastic differential equations, Springer-Verlag, Berlin, 1992.
[16] H.J. Kushner and P. Dupuis, Numerical methods for stochastic control problems in continuous time, Springer-Verlag, Berlin, 2001.
[17] G.N. Milstein, Numerical Integration of Stochastic Differential Equations, Kluwer Academic Publishers, Dordrecht, 1995.
[18] G.N. Milstein, The probability approach to numerical solution of nonlinear parabolic equations, Numer. Methods Partial Differential Equations, 18 (2002), 490–522.
[19] G.N. Milstein and M.V. Tretyakov, Numerical algorithms for semilinear parabolic equations with small parameter based on approximation of stochastic equations, Math. Comp., 69 (2000), 237–267.
[20] G.N. Milstein and M.V. Tretyakov, Numerical solution of the Dirichlet problem for nonlinear parabolic equations by a probabilistic approach, IMA J. Num. Anal., 21 (2001), 887–917.
[21] K.W. Morton, A. Priestley and E. Süli, Stability of the Lagrange-Galerkin method with non-exact integration, RAIRO Model. Math. Anal. Numer., 22 (1988), 625–653.
[22] O. Pironneau, On the transport-diffusion algorithm and its applications to the Navier-Stokes equations, Num. Math., 38 (1982), 309–332.
[23] A. Robert, A stable numerical integration scheme for the primitive meteorological equations, Atmos. Ocean., 19 (1981), 35–46.
[24] E. Sonnendrücker, J. Roche, P. Bertrand and A. Ghizzo, The semi-Lagrangian method for the numerical resolution of the Vlasov equation, J. Comput. Phys., 149 (1999), 201–220.
[25] A. Staniforth and J. Coté, Semi-Lagrangian integration schemes for atmospheric models - a review, Monthly Weather Review, 119 (1991), 2206–2223.
[26] A. Wiin-Nielsen, On the application of trajectory methods in numerical forecasting, Tellus, 11 (1959), 180–196.
[27] J. Zhang, Rate of convergence of finite difference approximations for degenerate ordinary differential equations, Math. Comp., 75 (2006), 1755–1778.